

Simulation of single diffraction dissociation in resonance region at LHC energies

O. S. Potiienko¹, D. V. Zhuravel², D. M. Riabov³, and N. O. Chudak¹

¹Odesa Polytechnic National University, Shevchenko av. 1, Odesa, 65044, Ukraine

²Bogolyubov Institute for Theoretical Physics (BITP), National Academy of Sciences of Ukraine, Metrolohichna st. 14-b, Kiev, 03143, Ukraine

³State University of Intellectual Technologies and Communications, Kuznechna st. 1, Odesa, 65023, Ukraine

November 27, 2024

Abstract

A comprehensive review of the single diffraction dissociation duality-based model at low missing masses have been presented. The distinguishing feature of the model is the nonlinear Regge proton trajectory used to account for the resonances contributions to the cross-sections. It helps classify and understand the spectrum of excited states of proton and their decays, providing insights into the internal structure and dynamics of particles. The behavior of the differential cross-section in the resonance region at small missing masses M_x is investigated. The model parameters are refined in the light of new experimental data.

1 Introduction

As is known from many experimental results [1], in the processes of hadron scattering at high energies, the majority of events are concentrated in the region of small momentum transfers. The combination of high energies and small momentum transfers creates conditions for the realization of diffraction processes [2, 3]. Diffraction in particle physics draws an analogy from classical wave diffraction, where waves encounter an obstacle and spread out. Similarly, in diffractive dissociation, a hadron such as a proton encounters another particle or nucleus, leading to its partial or complete dissociation. The process is characterized by a small momentum transfer between the incident particle and the target, resulting in a "rapidity gap" – a region in the detector with very few or no particles. One of the significant findings from diffractive dissociation studies is the confirmation of the pomeron exchange model, which has been supported by experimental data showing characteristic rapidity gaps in diffractive events. The detailed measurements of diffractive cross-sections and the kinematic distributions of final-state particles have provided insights into the non-perturbative aspects of QCD.

The main types of diffractive processes are single dissociation (SD), double dissociation (DD), and central diffraction (CD) (Fig. 1). Diffraction dissociation has been studied in various high-energy physics experiments, such as TOTEM [4], CMS [5], CERN [6–8], ALICE [9] and ATLAS [10]. In this work, we consider the low-mass single diffraction dissociation of protons. The small missing masses M_X show a multitude of peaks or features corresponding to different nucleon resonances [11]. Nucleon resonances are essential for understanding the strong force interactions described by QCD.

The experimentally observed characteristics of the diffraction dissociation largely depend on the properties of the hadron-region vertex. We will consider this vertex as the amplitude of a real process. Using the unitarity condition [12], duality [13], this amplitude can be calculated as the sum of the resonance contributions known from experiments [14]. In this work, we examined the exchange of a single pomeron. This pomeron is typically considered to be a simple pole of the partial scattering amplitude. However, there are other dynamic models, such as the model with exchange of a pomeron-like analog but with an odd signature [15, 16], and the dipole pomeron model, which is the foundation,

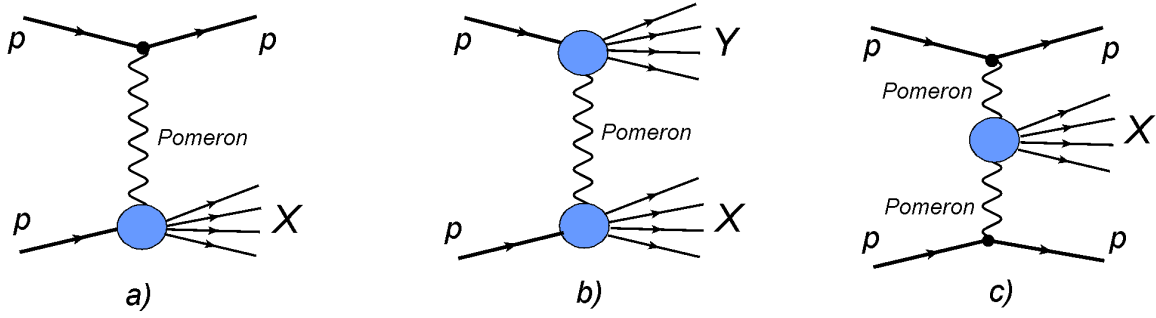


Figure 1: The main types of diffractive processes: a) single dissociation (SD), b) double dissociation (DD) and c) central diffraction (CD), where p - is proton, $X(Y)$ - is a system of secondary hadrons.

further enhanced by incorporating a dip-bump mechanism [17]. Therefore, it is interesting to explore the combination of different models of the hadron-reggeon vertex and collision dynamics to describe experimental data. In this work, we present the results of fits with the exchange of a single pomeron pole.

Our goal is to calculate the differential cross-section $d\sigma/dt$ of single diffraction dissociation within the resonance region at small missing masses M_X and the total single diffraction dissociation cross section.

The structure of the article is presented as follows. In Section 2 we find the structure function of proton $W_2(M_X^2, t)$, which related to the imaginary part of dual-Regge transition amplitude $A(M_X^2, t)$. In Section 3 we show that the behavior of the cross-section is influenced by baryon resonances. In Section 4 we calculate total and differential cross-sections and fit them to the experimental data.

2 From elastic scattering to single diffractive dissociation

Let us consider the diffractive dissociation $p + p \rightarrow p + X$, where p is a proton, X is a system of secondary hadrons. This process is represented as a similar elastic process, where X is considered as a single particle with a squared mass M_X^2 , which equals the scalar square of the sum of the four-momenta of X . Then, instead of the elastic scattering amplitude we obtain the amplitude of diffractive dissociation with the vertices of the reggeon-hadron interaction. Such modification [11] leads to the expression (1) for the differential cross-section of single diffraction dissociation at large s (the square of the center-of-mass energy of the collision)

$$\frac{d\sigma_{SD}}{dt dM_X^2} \approx \frac{9\beta^4}{4\pi} [F^p(t)]^2 \left(\frac{s}{M_X^2} \right)^{2(\alpha_P(t)-1)} \frac{W_2(t, M_X^2)}{2m}, \quad (1)$$

where t is the momentum transfer between colliding particles, β is the quark-Pomeron coupling, m is proton mass, $\alpha_P(t)$ is a vacuum Regge trajectory, $F^p(t)$ is elastic form factor of proton, $W_2(t, M_x^2)$ is a structure function of proton, which describes the Pomeron-proton vertex. According to [11, 18] we take the Pomeron trajectory $\alpha_P(t) = 1.08 + 0.25t$. The expression for the proton elastic form factor is given by $F^p(t) = (1.0 - t/0.71)^{-2}$.

The most challenging building block of the expression (1) is the structure function $W_2(t, M_x^2)$.

Following [11], this structure function can be constructed from the similarity between the Pomeron-proton diffractive process $\mathbb{P}p \rightarrow X$ (Pomeron denoted by \mathbb{P}) and deeply virtual Compton scattering process $\gamma^*p \rightarrow X$ (Fig. 2). Let us briefly highlight the major steps on the way to $W_2(M_X^2, t)$:

Step 1: Similarity with $\gamma^*p \rightarrow X$

We utilize the similarity between the inelastic vertices $\mathbb{P}p \rightarrow X$ and $\gamma^*p \rightarrow X$ and the corresponding structure functions. The structure functions $F_2(x, Q^2)$ for γ^*p processes has been studied in [19], and are connected [20] with W_2 through the following relation

$$\nu W_2(M_X^2, t) = F_2(x, t), \quad (2)$$

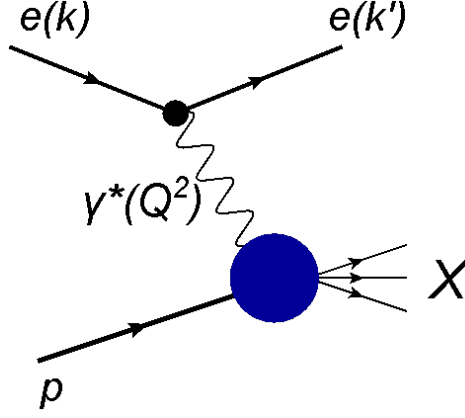


Figure 2: Deeply virtual Compton scattering process $\gamma^* p \rightarrow X$ transition

where $\nu = (M_X^2 - m^2 - t) / 2m$ is another kinematic variable. Thus, establishing an analogy between the virtual photon γ^* and the Pomeron (\mathbb{P}), and setting $Q^2 = -t$, yields

$$\nu W_2(M_X^2, t) = F_2(x, t) = \frac{-4t(1-x)^2}{\alpha_{fs}(M_X^2 - m^2)(1 - 4m^2x^2/t)^{3/2}} \text{Im } A(M_X^2, t), \quad (3)$$

where α_{fs} is fine structure constant, $x = -t/2m\nu$ is Bjorken variable, and $A(M_X^2, t)$ is the dual-Regge transition amplitude.

Step 2: Dual-Regge amplitude

The amplitude $A(M_X^2, t)$ in eq. (3) is obtained from unitarity and Veneziano duality [11]. According to the model of dual amplitude with Mandelstam analyticity (DAMA), the amplitude is expressed as the sum over Regge trajectories, ending up with the direct channel resonance decomposition

$$A(M_X^2, t) = a \sum_{n \geq 0} \frac{[f(t)]^{2(n+1)}}{2n + 0.5 - \alpha(M_X^2)}, \quad (4)$$

where a is normalization factor, $f(t) = (1 - t/t_0)^{-2}$ is the form factor of $\mathbb{P}p \rightarrow \mathbb{P}p$ system, t_0 is the model parameter. Finally, $\alpha(M_X^2)$ is the (nonlinear complex) baryonic resonance trajectory in M_X^2 channel, which allows to account for a set of various resonances.

The imaginary part of the amplitude (4) needed for structure function (3) is given by

$$\text{Im } A(M_X^2, t) = a \sum_{n \geq 0} [f(t)]^{2(n+1)} \frac{\text{Im } \alpha(M_X^2)}{[2n + 0.5 - \text{Re } \alpha(M_X^2)]^2 + [\text{Im } \alpha(M_X^2)]^2}. \quad (5)$$

Step 3: Proton trajectory

The last step in this journey is the nonlinear complex proton Regge trajectory $\alpha(M_X^2)$. It helps classify and understand the spectrum of excited states of proton and their decays, providing insights into the internal structure and dynamics of particles. These resonances indicate specific energy and angular momentum states where the proton can undergo transitions to excited states before returning to the ground state. The real part of the trajectory $\text{Re } \alpha(M_X^2)$ provides the relation between the mass of resonance and its angular momentum (quantum number J). At the same time, the imaginary part of the trajectory provides the Breit-Wigner widths of the resonances

$$\Gamma = \frac{\text{Im } \alpha(M^2)}{M \text{Re } \alpha'(M^2)}, \quad (6)$$

where M is the resonance mass, $\text{Re } \alpha'(M^2)$ denotes the first derivative (the slope) of the real part of trajectory. The problem is to find a trajectory $\alpha(M^2)$ featuring both the almost linear real part

(Fig. 3a) and essentially nonlinear imaginary part (Fig. 3b), while holding the analyticity properties. Such trajectory has been extensively studied in [21] with the help of dispersion relations, which provides us with the expressions

$$\mathcal{Im} \alpha(s) = s^\delta \sum_n c_n \left(\frac{s - s_n}{s_n} \right)^{\mathcal{Re} \alpha(s_n)} \theta(s - s_n), \quad (7)$$

$$\mathcal{Re} \alpha(s) = \alpha(0) + \frac{s}{\pi} \sum_n c_n \mathcal{A}_n(s), \quad (8)$$

where c_n and s_n are parameters to be fitted using the experimental data on resonances widths and masses, $\alpha(0)$ is the intercept of the real part of trajectory. Note, that hereinafter the quantities s and s_n are nondimensionalized by $s_0 = 1$ GeV, so that resulting expressions are dimensionless, e.g. (7) and (8). The Heaviside step function $\theta(\cdot)$ is conventionally defined such that $\theta(0) = \frac{1}{2}$. The term $\mathcal{A}_n(s)$ in (8) emerges from a dispersion relation and is given by

$$\begin{aligned} \mathcal{A}_n(s) = & \frac{\Gamma(1-\delta)\Gamma(\lambda_n+1)}{\Gamma(\lambda_n-\delta+2)} s_n^{\delta-1} {}_2F_1 \left(1, 1-\delta; \lambda_n-\delta+2; \frac{s}{s_n} \right) \theta(s_n - s) + \\ & \left\{ \pi s^{\delta-1} \left(\frac{s-s_n}{s} \right)^{\lambda_n} \cot[\pi(1-\delta)] - \right. \\ & \left. \frac{\Gamma(-\delta)\Gamma(\lambda_n+1)}{\Gamma(\lambda_n-\delta+1)} \left(\frac{s_n^\delta}{s} \right) {}_2F_1 \left(\delta - \lambda_n, 1; \delta + 1; \frac{s_n}{s} \right) \right\} \theta(s - s_n), \end{aligned} \quad (9)$$

where δ is the dimensionless parameter to be fitted, $\Gamma(x)$ is the gamma function, ${}_2F_1(a, b; c, z)$ is the Gaussian hypergeometric function, $\cot(x)$ denotes cotangent function, and $\lambda_n = \mathcal{Re} \alpha(s_n)$.

Note that $\mathcal{Re} \alpha$ appear on the both sides of equation (8) through λ_n . Thus, (7), (8) and (9) are in fact functional equations, which significantly sophisticates the fitting procedure necessary to determine the value of parameters $\alpha(0)$, δ , c_n , and s_n , where $n = 1, 2, x$.

The baryons included in the trajectory are N(939), N(1680), N(2220), N(2700) and their properties depicted in Tab. 1. These resonances have been observed in experiments studying single diffraction dissociation processes, providing a framework for the study of SDD. The recursive fitting procedure of proton trajectory (7), (8) to the data for these resonances has been performed in [21].

Name	J	M (MeV)	Γ (MeV)
N(939)	1/2	939	—
N(1680)	5/2	1684 ± 4	128 ± 8
N(2220)	9/2	2230 ± 80	400 ± 150
N(2700)	13/2	2612 ± 45	350 ± 50

Table 1: The baryons included in the fit [21] of trajectory $\alpha(s)$. The columns from left to right are: the baryon name, total angular momentum J , Breit-Wigner mass M , Breit-Wigner width Γ .

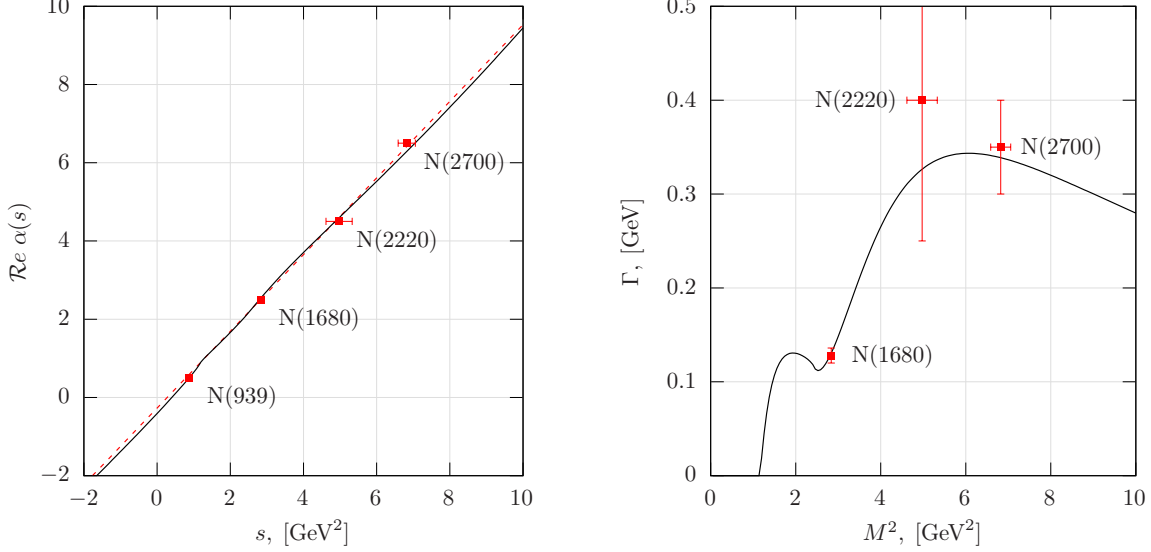
The fitting algorithm can be summarized as follows. Due to the close-to-linear form of the real part of trajectory, it is reasonable to start with the fit of the linear approximation of the real part $\alpha_{lin}(s) = \alpha(0) + \alpha'(0)s$, which gives the initial values of $\lambda_n^{(0)} = \mathcal{Re} \alpha_{lin}(s_n)$. Then, the expression (6) for the widths of resonances is iteratively fitted to the experimental data Tab. 1. After each iteration, the values of λ_n are updated $\lambda_n = \mathcal{Re} \alpha(s_n)$ using (8) with the updated values of parameters. The process is repeated until the sequence of trajectories converges. The resulting values of parameters are summarized in below in Tab. 2.

Using the values of parameters from Tab. 2 we plot the trajectory $\alpha(s)$ and ensure it match [21] (see Fig. 3). This completes the construction of the expression for differential cross-section for single diffraction dissociation (1).

Substituting W_2 from (3) into (1) we obtain

$\alpha(0) = -0.41$	$c_1 = 0.51$	$s_1 = 1.16 \text{ GeV}^2$
$\delta = -0.46$	$c_2 = 4.0$	$s_2 = 2.44 \text{ GeV}^2$
	$c_x = 4.6 \times 10^3$	$s_x = 11.7 \text{ GeV}^2$

Table 2: Parameters of proton trajectory $\alpha(s)$ obtained in [21] by fitting (6) to resonances data Tab. 1.



(a) The real part of fitted proton trajectory (8) (black solid line) and linear fit (red dashed line).

(b) The fit of resonance widths (6) (solid line) and experimental data from Tab. 1.

Figure 3: The fit [21] of the proton trajectory to N-resonances data.

$$\begin{aligned}
\frac{d^2\sigma}{dt dM_X^2}(M_X^2, t) &= A_0 \left(\frac{s}{M_X^2} \right)^{2\alpha_P(t)-2} \frac{x(1-x)^2 [F^p(t)]^2}{(M_X^2 - m^2)(1 - 4m^2x^2/t)^{3/2}} \\
&\times \sum_{n=1}^3 [f(t)]^{2(n+1)} \frac{\text{Im } \alpha(M_X^2)}{[2n + 0.5 - \text{Re } \alpha(M_X^2)]^2 + [\text{Im } \alpha(M_X^2)]^2},
\end{aligned} \tag{10}$$

where $A_0 = 9a\beta^4/\pi\alpha_{fs}$ is the normalization factor that combines the factors a and β from (1) and (5). Another free parameter is t_0 of the form-factor $f(t)$ appearing in the expression for the transition amplitude (4). The rest of parameters $\alpha(0), \delta, c_n, s_n$ ($n = 1, 2, x$) are fixed from trajectory fit Tab. 2. The values of A_0 and t_0 can be determined from the fit of the differential cross-section $d\sigma_{\text{SDD}}/dt$ and total cross-section σ_{SDD} . In the next section we analyze the behavior of the double differential cross-section (10) and discuss the applicability range of the model.

3 Model behavior in the resonance region

In the study of single diffraction dissociation processes the regions of small and large missing masses M_X offer distinct mechanisms of particle interactions. Here we focus on the small missing masses M_X , where the behavior of the cross-section is notably influenced by resonances within the structure functions. These resonances manifest as peaks in the cross-section data, shaping the scattering processes observed at lower energies. In the present model, the resonances are accounted via proton trajectory described in the previous section. This trajectory defines the behavior of the differential cross-section (10) in the M_X region where resonances appear Fig. 4. As $M_X \rightarrow m$, the scattering process exhibits elastic-like nature (m is the proton mass), which significantly differs from the resonance production processes. The proper account for the contributions from the elastic and close-to-elastic processes requires a

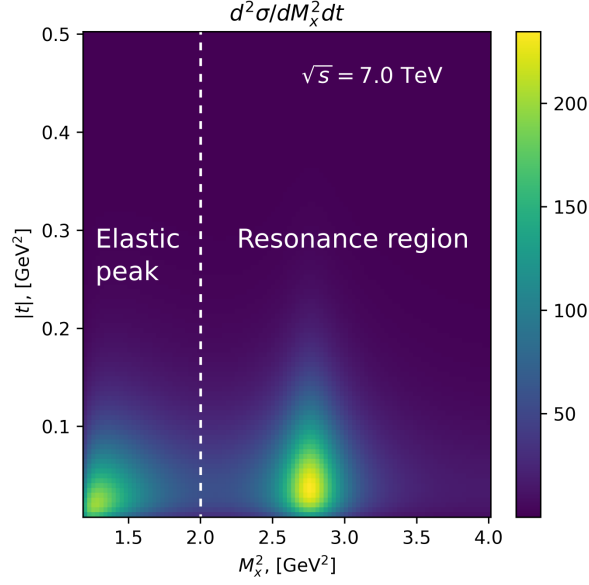


Figure 4: The differential cross-section $d^2\sigma/dtdM_X^2$ (10) in t , M_X^2 plane. There are two missing mass M_X regions: elastic peak region ($M_X^2 < 2 \text{ GeV}^2$), and the resonance region ($2 \text{ GeV}^2 \leq M_X^2 \leq 8 \text{ GeV}^2$).

distinct model. Thus we focus on the contributions from the resonance region only and *consider elastic processes as background contributions*. In the present model the elastic contributions appear as the elastic peak in the differential cross-section as low M_X , as can be seen in Fig. 4. To avoid double counting in the elastic region, we follow [11] and consider $M_X^2 \geq 2 \text{ GeV}^2$, which cuts elastic peak off. At the same time, at large missing masses M_X , the contributions of resonance productions expectedly reduce, making cross-section (10) neglectedly small for $M_X^2 > 8 \text{ GeV}^2$. In this region another Regge mechanisms come into play, but they are outside of the scope of the present work. This justifies what we call the *resonance region* $2 \text{ GeV}^2 \leq M_X^2 \leq 8 \text{ GeV}^2$.

The plots of double differential cross-section (10) in the resonance region are depicted on Figs. 5, 6, 7. The single peak in M_X^2 dimension is clearly visible in the resonance region. The unfitted values of parameters used in this section are $A_0 = 10^3 \text{ mb/GeV}^2$ and $t_0 = 0.71 \text{ GeV}^2$.

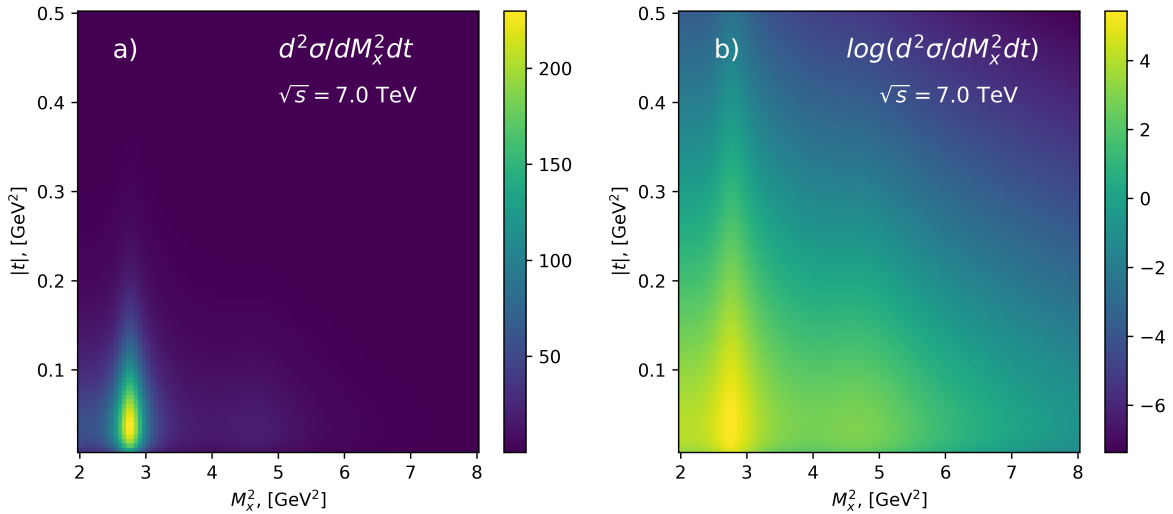


Figure 5: The differential cross-section $d^2\sigma/dtdM_X^2$ (10) in the t , M_X^2 plane (a), and its logarithm (b), plotted in the resonance region for $0 \leq -t \leq 0.5 \text{ GeV}^2$.

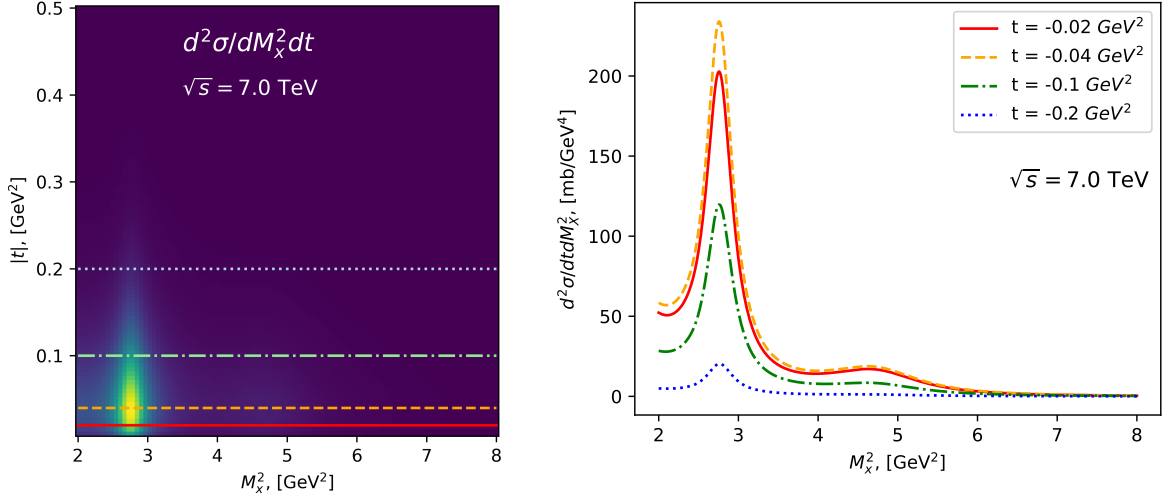


Figure 6: The differential cross-section $d^2\sigma/dtdM_X^2$ (10) in the t , M_X^2 plane in the resonance region for $0 \leq -t \leq 0.5$ GeV^2 (left), and multiple regular plots in M_X^2 at fixed values of t (right).

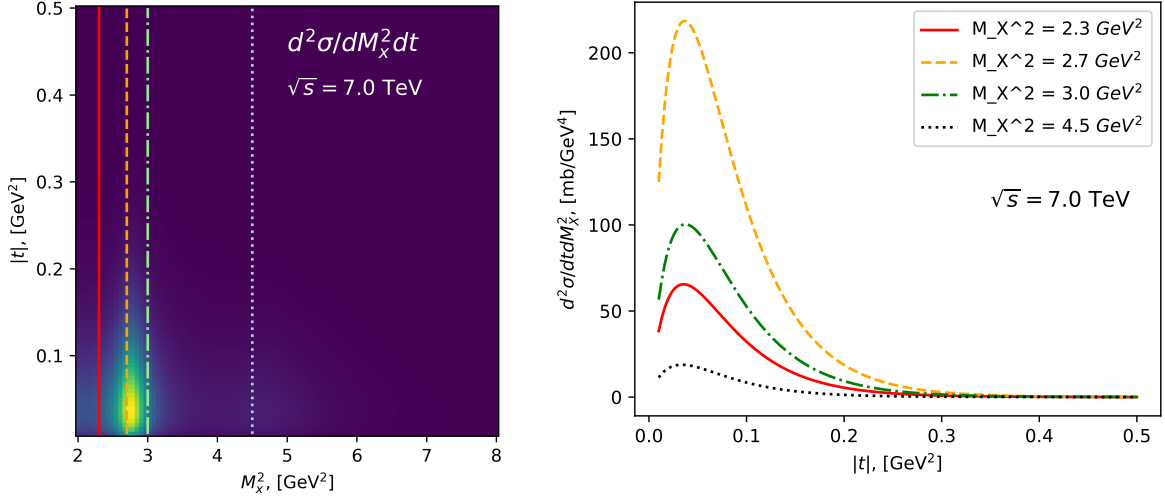


Figure 7: The differential cross-section $d^2\sigma/dtdM_X^2$ (10) in the t , M_X^2 plane in the resonance region for $0 \leq -t \leq 0.5$ GeV^2 (left), and multiple regular plots in t at fixed values of M_X^2 (right).

4 Cross-sections

In this section we calculate total and differential cross-sections and fit them to the experimental data to find the values of parameters A_0 and t_0 .

First, we integrate the double differential cross-section (10) over M_X^2 in resonance region to calculate the differential cross-section

$$\frac{d\sigma}{dt}(t) = \int_2^8 \frac{d^2\sigma}{dt dM_X^2}(t, M_X^2) dM_X^2 + b_0, \quad (11)$$

where b_0 is the simple model of background contribution discussed in the previous section. Then we fit (11) to the experimental data [10] using the ROOT implementation of Minuit framework. The fitting procedure converges with $\chi^2/d.o.f. \approx 1.07$, providing the following values of parameters: $A_0 = 35.58$ mb/GeV^2 , $t_0 = 1.486$ GeV^2 , and $b_0 = 8.2$ mb/GeV^2 . The result of fitting procedure is shown in Fig. 8.

The next step, is to integrate 11 over $t \in [0, 0.5]$ to calculate the total cross-section

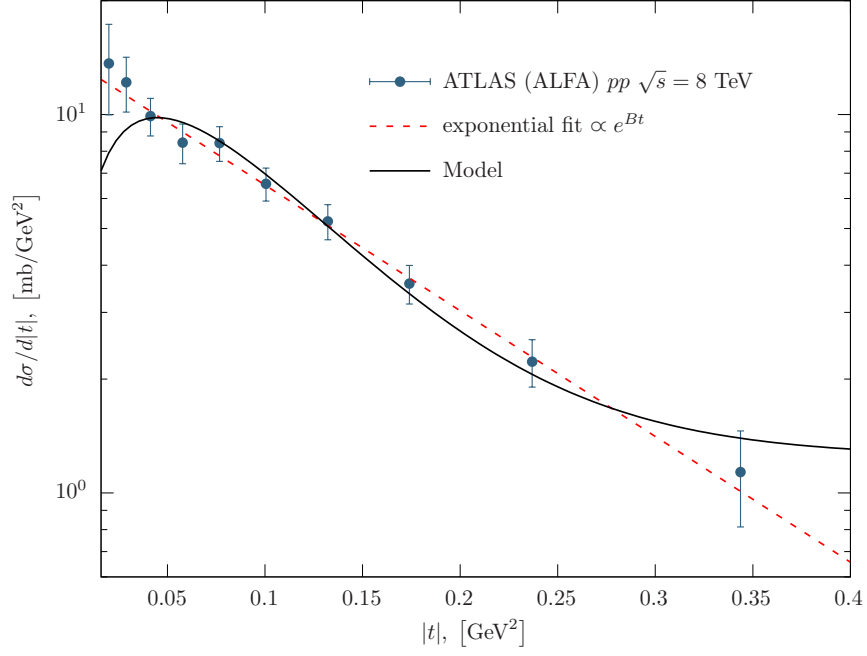


Figure 8: The differential cross-section $d\sigma/dt$ of single diffraction dissociation as a function of $|t|$. The dashed line is the exponential fit to the experimental data [10]. The solid line is the model fit with the constant background contribution b_0 .

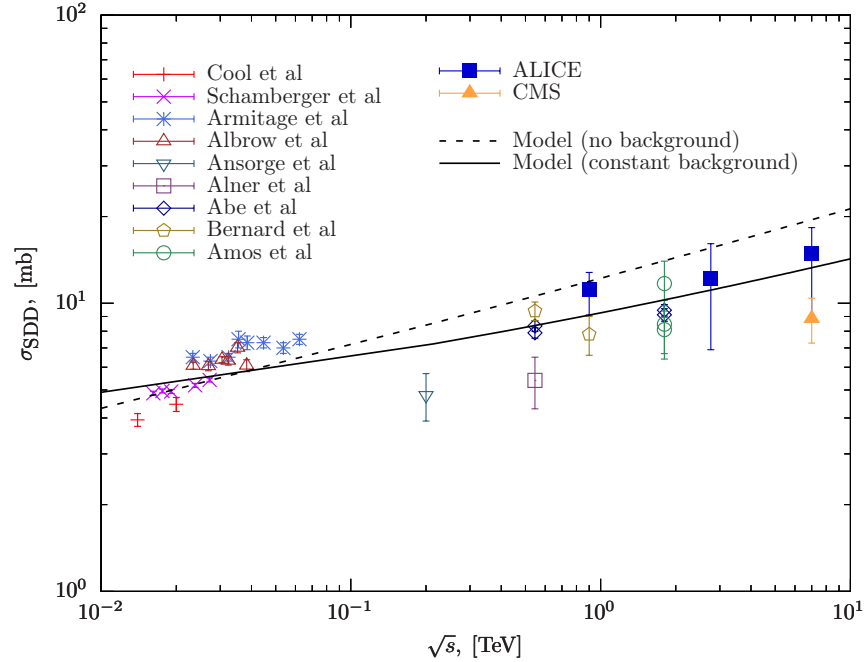


Figure 9: The total single diffraction dissociation cross-section as a function of \sqrt{s} . The dashed line is the model fit to the experimental data [5–9, 22–28] without any background contribution. The solid line is the fit with the constant background contribution b .

$$\sigma_{\text{SDD}} = \int_{-s}^0 \int_2^8 \frac{d^2\sigma}{dt dM_X^2} (t, M_X^2) dM_X^2 dt + b, \quad (12)$$

where b is the background contribution. Note, that we do not have any reliable model for the background, so we relax the connection between b_0 and b and fit them separately. The fit of differential cross-section $d\sigma/dt$ gives us the reasonable estimate for $t_0 = 1.486 \text{ GeV}^2$ that we can use in total cross-section fit. The fitting procedure converges giving $\chi^2/d.o.f. = 14.03$ without background contribution, and providing the value of $A_0 = 565 \pm 3.11 \text{ mb/GeV}^2$. Accounting for the constant background contribution b , gives us better fit result $\chi^2/d.o.f. = 10.72$. The values of parameters in this case are $A_0 = 378.43 \pm 16.68 \text{ mb/GeV}^2$ and $b = 1.85 \pm 0.16 \text{ mb/GeV}^2$.

5 Low missing mass event generation

The differential cross-sections fitted in the previous section provide facilities to generate events for low missing mass single diffractive processes.

In this context, the four-momentum transfer squared t and the squared mass M_X^2 of the dissociated system become random variables. The joint probability density of t and M_X^2 is given by the double differential cross-section (10) at fixed \sqrt{s}

$$\rho(M_X^2, t) = \frac{1}{N} \frac{d^2\sigma}{dt dM_X^2}(M_X^2, t), \quad (13)$$

where $N = \sigma_{SD}(\sqrt{s})$ is the normalizing factor ensuring unit total probability, and $\sigma_{SD}(\sqrt{s})$ is the integrated single diffraction dissociation cross-section (12). As discussed in the previous section, we consider the domain of $M_X^2 \in [2, 8] \text{ GeV}^2$.

To generate an event we sample a pair (t, M_X^2) from the probability density (15). While this can be done in multiple ways (e.g. the acceptance-rejection method [29]), we follow the algorithm used in the Minimum Bias Rockefeller (MBR) simulation [30] implemented in Pythia 8 event generator. The idea is to begin by sampling a value of M_X^2 from the marginal probability density function

$$\rho_{M_X}(M_X^2) = \int_{t_{min}}^0 \rho(M_X^2, t) dt = \frac{1}{N} \int_{t_{min}}^0 \frac{d^2\sigma}{dt dM_X^2}(M_X^2, t) dt, \quad (14)$$

where $t_{min} = -1 \text{ GeV}^2$ defines the integration lower bound, cutting off the region of the small values of cross-section. The integral in (14) is calculated numerically.

Next, the value of t is sampled from the conditional probability density function

$$\rho_t(t | M_X^2) = \frac{\rho(M_X^2, t)}{\rho_{M_X}(M_X^2)}. \quad (15)$$

Finally, the generated pair (t, M_X^2) together with the Mandelstam variable s gives us the four-momenta of the proton and dissociated system in the final state, which can be calculated from the relativistic kinematics of two-body scattering.

To compare our results against the MBR approach, alongside with kinematic variable M_X^2 we consider the rapidity gap $\eta = -\log(M_X^2/s)$. In this variable, the low missing mass region $M_X^2 \in [2, 8] \text{ GeV}^2$ corresponds to the interval $15.6 \leq \eta \leq 17$ at $\sqrt{s} = 7 \text{ TeV}$. Despite this interval is quite narrow compared to the $0 \leq \eta \leq 17.5$ in [30], it exhibits a significant difference between two approaches. The MBR simulation demonstrates the close to constant behavior of the cross-section in the region of low missing masses. Whereas our model predicts highly non-monotonical dependency with multiple peaks corresponding to the resonances.

6 Summary

The in-depth examination of the differential cross-sections behavior within the resonance region is performed, particularly at low missing masses M_X . The refinement of model parameters through the incorporation of new experimental data is discussed, improving accuracy and predictive capabilities. The fits of differential and total cross-sections were performed using C++ programs within the ROOT framework, specifically employing Minuit for parameter optimization. Results are presented as numerical values of parameters, goodness-of-fit metrics, and graphical representations, providing a clear

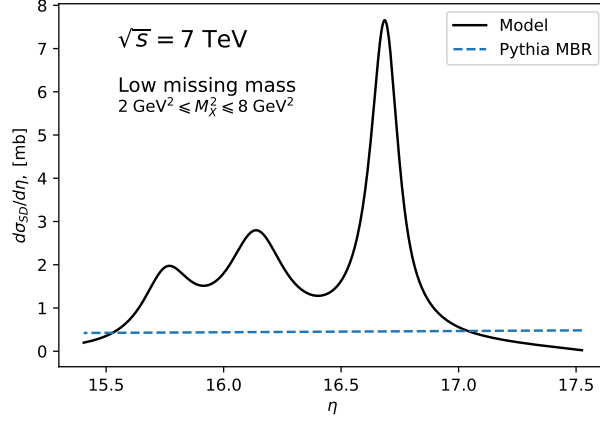


Figure 10: The comparison of the our model against the MBR simulation in Pythia 8 at $\sqrt{s} = 7$ TeV.

and comprehensive depiction of the model performance. The constant background contribution b was assumed due to the lack of a refined model for background effects. The proper modeling of background contributions could potentially yield significant improvements in the accuracy of results and should be a focus of future research.

Acknowledgments

This project has received funding through the EURIZON project, which is funded by the European Union under grant agreement No.871072.

References

- [1] Konstantin A. Goulianos. Diffractive Interactions of Hadrons at High-Energies. *Phys. Rept.*, 101: 169, 1983. doi: 10.1016/0370-1573(83)90010-8.
- [2] E Feinberg and I Pomeranchuk. Nuovo cimento. *Suppl.*, 3:652, 1956.
- [3] M. L. Good and W. D. Walker. Diffraction dissciation of beam particles. *Phys. Rev.*, 120: 1857–1860, 1960. doi: 10.1103/PhysRev.120.1857.
- [4] G. Antchev et al. Double diffractive cross-section measurement in the forward region at the lhc. *Phys. Rev. Lett.*, 111:262001, Dec 2013. doi: 10.1103/PhysRevLett.111.262001. URL <https://link.aps.org/doi/10.1103/PhysRevLett.111.262001>.
- [5] V. Khachatryan et al. Measurement of diffractive dissociation cross sections in pp collisions at $\sqrt{s} = 7$ TeV. *Phys. Rev. D*, 92:012003, Jul 2015. doi: 10.1103/PhysRevD.92.012003. URL <https://link.aps.org/doi/10.1103/PhysRevD.92.012003>.
- [6] M.G. Albrow, A. Bagchus, D.P. Barber, P. Benz, A. Bogaerts, B. Bösnjaković, J.R. Brooks, C.Y. Chang, A.B. Clegg, F.C. Ern , C.N.P. Gee, P. Kooijman, D.H. Locke, F.K. Loebinger, N.A. McCubbin, P.G. Murphy, D. Radoj i , A. Rudge, J.C. Sens, A.L. Sessoms, J. Singh, D. Stork, and J. Timmer. Inelastic diffractive scattering at the cern isr. *Nuclear Physics B*, 108(1):1–29, 1976. ISSN 0550-3213. doi: [https://doi.org/10.1016/0550-3213\(76\)90121-8](https://doi.org/10.1016/0550-3213(76)90121-8). URL <https://www.sciencedirect.com/science/article/pii/0550321376901218>.
- [7] R. E. Ansorge et al. Diffraction Dissociation at the CERN Pulsed Collider at CM Energies of 900-GeV and 200-GeV. *Z. Phys. C*, 33:175, 1986. doi: 10.1007/BF01411134.

- [8] D. Bernard, M. Bozzo, P.L. Braccini, F. Carbonara, R. Castaldi, F. Cervelli, G. Chiefari, E. Drago, M. Haguenaue, V. Innocente, P. Kluit, B. Koene, S. Lanzano, G. Matthiae, L. Merola, M. Napolitano, V. Palladino, G. Sanguinetti, P. Scampoli, S. Scapellato, G. Sciacca, G. Sette, R. Van Swol, J. Timmermans, C. Vannini, J. Velasco, P.G. Verdini, and F. Visco. The cross section of diffraction dissociation at the cern sps collider. *Physics Letters B*, 186(2): 227–232, 1987. ISSN 0370-2693. doi: [https://doi.org/10.1016/0370-2693\(87\)90285-1](https://doi.org/10.1016/0370-2693(87)90285-1). URL <https://www.sciencedirect.com/science/article/pii/0370269387902851>.
- [9] B. Abelev et al. Measurement of inelastic, single- and double-diffraction cross sections in proton–proton collisions at the lhc with alice. *The European Physical Journal C*, 73(6), June 2013. ISSN 1434-6052. doi: 10.1140/epjc/s10052-013-2456-0. URL <http://dx.doi.org/10.1140/epjc/s10052-013-2456-0>.
- [10] G Aad and The ATLAS collaboration. Measurement of differential cross sections for single diffractive dissociation in $\sqrt{s} = 8$ TeV pp collisions using the ATLAS ALFA spectrometer. *J. High Energy Phys.*, 2020(2), February 2020.
- [11] L. L. Jenkovszky, O. E. Kuprash, J. W. Lamsa, V. K. Magas, and R. Orava. Dual-regge approach to high-energy, low-mass diffraction dissociation. *Phys. Rev. D*, 83:056014, Mar 2011. doi: 10.1103/PhysRevD.83.056014. URL <https://link.aps.org/doi/10.1103/PhysRevD.83.056014>.
- [12] M. Baker and K.A. Ter-Martirosyan. Gribov’s reggeon calculus: Its physical basis and implications. *Physics Reports*, 28(1):1–143, 1976. ISSN 0370-1573. doi: [https://doi.org/10.1016/0370-1573\(76\)90002-8](https://doi.org/10.1016/0370-1573(76)90002-8). URL <https://www.sciencedirect.com/science/article/pii/0370157376900028>.
- [13] P. D. B. Collins. *An Introduction to Regge Theory and High Energy Physics*. Cambridge Monographs on Mathematical Physics. Cambridge University Press, 7 2023. ISBN 978-1-00-940326-9, 978-1-00-940329-0, 978-1-00-940328-3, 978-0-521-11035-8. doi: 10.1017/9781009403269.
- [14] K. Hagiwara et al. Review of particle properties. *Phys. Rev. D*, 66:010001, Jul 2002. doi: 10.1103/PhysRevD.66.010001. URL <https://link.aps.org/doi/10.1103/PhysRevD.66.010001>.
- [15] Laszlo Jenkovszky, Rainer Schicker, and Istvan Szanyi. Elastic and diffractive scatterings in the LHC era. *Int. J. Mod. Phys. E*, 27(08):1830005, 2018. doi: 10.1142/S0218301318300059.
- [16] Istvan Szanyi, Laszlo Jenkovszky, Rainer Schicker, and Volodymyr Svintozelskyi. Pomeron/glueball and odderon/oddball trajectories. *Nucl. Phys. A*, 998:121728, 2020. doi: 10.1016/j.nuclphysa.2020.121728.
- [17] Laszlo Jenkovszky, Rainer Schicker, and Istvan Szanyi. Dip-Bump Structure in Proton’s Single Diffractive Dissociation at the Large Hadron Collider. *Universe*, 10(5):208, 2024. doi: 10.3390/universe10050208.
- [18] Sandy Donnachie, Gunter Dosch, Peter Landshoff, and Otto Nachtmann. *Pomeron Physics and QCD*. Cambridge Monographs on Particle Physics, Nuclear Physics and Cosmology. Cambridge University Press, 2002.
- [19] R. Fiore, A. Flachi, L. L. Jenkovszky, A. I. Lengyel, and V. K. Magas. Kinematically complete analysis of the clas data on the proton structure function F_2 in a regge-dual model. *Phys. Rev. D*, 69:014004, Jan 2004. doi: 10.1103/PhysRevD.69.014004. URL <https://link.aps.org/doi/10.1103/PhysRevD.69.014004>.
- [20] Francis Halzen and Alan D Martin. *Quarks and leptons*. John Wiley & Sons, Nashville, TN, January 1984.
- [21] R. Fiore, L. L. Jenkovszky, F. Paccanoni, and A. Prokudin. Baryonic regge trajectories with analyticity constraints. *Phys. Rev. D*, 70:054003, Sep 2004. doi: 10.1103/PhysRevD.70.054003. URL <https://link.aps.org/doi/10.1103/PhysRevD.70.054003>.

- [22] R. L. Cool, K. Goulios, S. L. Segler, H. Sticker, and S. N. White. Diffraction dissociation of π^\pm , K^\pm , and p^\pm at 100 and 200 gev/c. *Phys. Rev. Lett.*, 47:701–704, Sep 1981. doi: 10.1103/PhysRevLett.47.701. URL <https://link.aps.org/doi/10.1103/PhysRevLett.47.701>.
- [23] R. D. Schamberger, J. Lee-Franzini, R. McCarthy, S. Childress, and P. Franzini. Mass spectrum of proton-proton inelastic interactions from 55 to 400 gev/c at small momentum transfer. *Phys. Rev. D*, 17:1268–1291, Mar 1978. doi: 10.1103/PhysRevD.17.1268. URL <https://link.aps.org/doi/10.1103/PhysRevD.17.1268>.
- [24] J.C.M. Armitage, P. Benz, G.J. Bobbink, F.C. Erne, P. Kooijman, F.K. Loebinger, A.A. Macbeth, H.E. Montgomery, P.G. Murphy, A. Rudge, J.C. Sens, D. Stork, and J. Timmer. Diffraction dissociation in proton-proton collisions at isr energies. *Nuclear Physics B*, 194(3): 365–372, 1982. ISSN 0550-3213. doi: [https://doi.org/10.1016/0550-3213\(82\)90014-1](https://doi.org/10.1016/0550-3213(82)90014-1). URL <https://www.sciencedirect.com/science/article/pii/0550321382900141>.
- [25] G.J. Alner, K. Alpgard, P. Anderer, R.E. Ansorge, B. Asman, S. Berglund, K. Berkelman, D. Bertrand, C.N. Booth, C. Buffam, L. Burow, P. Carlson, J.-L. Chevalley, C. Declercq, R.S. DeWolf, B. Eckart, G. Ekspong, I. Evangelou, A. Eyring, J.-P. Fabre, M. Fischer, K.A. French, C. Fuglesang, J. Gaudaen, C. Geich-Gimbel, M. Gijzen, K. von Holt, R. Hospes, D. Johnson, K. Jon-And, Th. Kokott, M. Langer, F. Lotse, R. Mackenzie, M.N. Maggs, R. Meinke, Th. Müller, H. Mulkens, D.J. Munday, A. Odian, J.E.V. Ovens, M. Rosenberg, J.G. Rushbrooke, H. Saarikko, T. Saarikko, H. Schmickler, F. Triantis, L. Van hamme, Ch. Walck, C.P. Ward, D.R. Ward, G. Weber, T.O. White, G. Wilquet, and N. Yamdagni. Ua5: A general study of proton-antiproton physics at $\sqrt{s}=546$ gev. *Physics Reports*, 154(5):247–383, 1987. ISSN 0370-1573. doi: [https://doi.org/10.1016/0370-1573\(87\)90130-X](https://doi.org/10.1016/0370-1573(87)90130-X). URL <https://www.sciencedirect.com/science/article/pii/037015738790130X>.
- [26] F. Abe et al. Measurement of p^-p single diffraction dissociation at $\sqrt{s}=546$ and 1800 gev. *Phys. Rev. D*, 50:5535–5549, Nov 1994. doi: 10.1103/PhysRevD.50.5535. URL <https://link.aps.org/doi/10.1103/PhysRevD.50.5535>.
- [27] N.A. Amos, C. Avila, W.F. Baker, M. Bertani, M.M. Block, D.A. Dimitroyannis, D.P. Eartly, R.W. Ellsworth, G. Giacomelli, B. Gomez, J.A. Goodman, C.M. Guss, A.J. Lennox, M.R. Mondardini, J.P. Negret, J. Orear, S.M. Pruss, R. Rubinstein, S. Sadr, J.C. Sanabria, S. Shukla, I. Veronesi, and S. Zucchelli. A luminosity-independent measurement of the pp total cross section at $\sqrt{s}=1.8$ tev. *Physics Letters B*, 243(1):158–164, 1990. ISSN 0370-2693. doi: [https://doi.org/10.1016/0370-2693\(90\)90973-A](https://doi.org/10.1016/0370-2693(90)90973-A). URL <https://www.sciencedirect.com/science/article/pii/037026939090973A>.
- [28] N.A. Amos, C. Avila, W.F. Baker, M. Bertani, M.M. Block, D.A. Dimitroyannis, D.P. Eartly, R.W. Ellsworth, G. Giacomelli, B. Gomez, J.A. Goodman, C.M. Guss, B. Hoeneisen, A.J. Lennox, M.R. Mondardini, J.P. Negret, J. Orear, S.M. Pruss, R. Rubinstein, S. Sadr, J.C. Sanabria, S. Shukla, M. Spagnoli, I. Veronesi, and S. Zucchelli. Diffraction dissociation in pp collisions at $\sqrt{s}=1.8$ tev. *Physics Letters B*, 301(2):313–316, 1993. ISSN 0370-2693. doi: [https://doi.org/10.1016/0370-2693\(93\)90707-O](https://doi.org/10.1016/0370-2693(93)90707-O). URL <https://www.sciencedirect.com/science/article/pii/037026939390707O>.
- [29] Luc Devroye. *Non-uniform random variate generation*. Springer, New York, NY, 1986 edition, April 1986.
- [30] Robert Ciesielski and Konstantin Goulios. MBR Monte Carlo Simulation in PYTHIA8. *PoS, ICHEP2012*:301, 2013. doi: 10.22323/1.174.0301.